Research Article

Discharge Structure of Ar/SF$_6$ Inductively Coupled Plasma at Relatively Low Pressures

Shu-Xia Zhao*

Key Laboratory of Material Modification by Laser, Ion, and Electron Beams (Ministry of Education), School of Physics, Dalian University of Technology, 116024, Dalian, China

Abstract:

The discharge structure in an electronegative Ar/SF$_6$ inductively coupled plasma is investigated in the article at low pressure, 10mTorr. Parabola profile in the electronegative plasma core is given by the fluid simulation, in accordance to the prediction of analytical theory. Except the ordinary sheath, the overall discharge is separated into the electronegative core and electropositive edge, which are connected by a dielectric-type double layer. This is a novel type of double layer, distinct from the previously reported ones that are found in the space plasma and triggered by stream instability. A self-coagulated density bump is observed stamping onto the parabolic basis at the chamber periphery along polar direction. In the core, the anion is obeyed to the Boltzmann's balance and the density profile of electron is flattened at its own and the anion Boltzmann balances. The discovered discharge structure in electronegative plasma by means of simulation and theory is important for people to better understand and utilize the laboratory plasmas

Keywords: Parabolic Profile Theory, Separated Discharges, Novel Type of Double Layer, Self-Coagulation, Electronegative Discharge Structure

Correspondence:

Shu-Xia Zhao, Key Laboratory of Material Modification by Laser, Ion, and Electron Beams (Ministry of Education), School of Physics, Dalian University of Technology, 116024, Dalian, China, ORCID: 0000-0001-9270-7465

INTRODUCTION

Structure refers to the profile of plasma parameter that includes but is not limited to the quantities of density, temperature, potential, charge density, species flux and velocity. The structure of gaseous discharge plasma generated in the laboratory is more investigated than the space plasma because it is a bounded plasma and specific distribution of plasma parameter is easily formed. Technically, this is called as Discharge Structure. This structure is important for people to understand the plasma since it is a steady state result of transport scheme and chemical reaction of plasma inside. A comprehensive understanding of the structure hence needs the support of details of the temporal evolution of plasma dynamic process, i.e., the interior plasma collective interaction.

It is difficult to study the discharge structure of electronegative plasma that contains one or more of oxygen, chlorine, fluorocarbon, fluorine-sulphur components, due to the anion interfere in the ambi-polar diffusion and chemical bulk loss of plasma species (Lichtenberg, 1994; Lichtenberg, 1997). The complex system is better to be studied by coupling the different researching methods, like the numerical simulation, analytical theory and experimental diagnosis. As we understand, the simulation provides the details of dynamic process, the analytical theory illuminates the behind physics, and finally the experiment verifies the findings.

Discharge stratification, i.e., the discharge separating into the electronegative core and electropositive edge, has been recognized before by the analytical theory (Lichtenberg, 1994; Lichtenberg, 1997; Economou, 2007; & Lampe, 2004) and experiment (Berezhnoj, 2000). It is the first time reported in the article that the self-consistent fluid simulation can capture the above discharge characteristic as well, in an Ar/SF$_6$ inductively coupled plasma. Moreover, the simulation reveals a double layer at the interface of the two sub-discharge regions. The double layer is famous concept and believed to play important role in the formation of aurora in the ionosphere (Albert, 1970). Hence, many beam experiments are carried out to examine the essence of double layer (Albert, 1970; & Quon, 1976),

and it is found to be excited by the stream instability (Quon, 1976). The early studies reveal many types of double layer (Coakley, 1978; Knorr, 1974; Chan, 1984; & Chan, 1986), such as the strong (Coakley, 1978; & Knorr, 1974), ionic acoustic (Chan, 1984), and currentless type (Chan, 1986). In addition, the double layer is found also existing in the laboratory plasma, through the theory analysis (Kolobov, 1998; Sheridan, 1999; & Kouznetsov, 1999). It is similar to the simulated double layer of our fluid model, but the mechanism is not unveiled. In particular, does it resemble to the aurora double layer? And what is its role in the discharge separation? Positive or passive? All these questions need to be answered for thoroughly understanding the separation.

In the electronegative core, the simulation shows a density bump of ions superposed on a parabolic profile. The parabola profile can be described by the parabola theory (Lichtenberg, 1994; & Lichtenberg, 1997), which has already been experimentally verified (Berezhnoj, 2000; & Kaga, 2001). The anion in the theory is assigned to satisfy the Boltzmann balance, under the anion room temperature. The electron is also the Boltzmann balanced, at the electron temperature. The electron density is spatially flattened at the balances, due to the substantial difference between the temperatures of anion and electron. In addition, the recombination loss of ions in the theory is approximated to be negligible. The two theory approximations are proven to be reasonable by the simulation. The density bump simulated is out of the scope of parabola theory. It is given by the self-coagulation behavior that is revealed by the fluid simulation of an Ar/O2 inductively coupled plasma in Reference (Zhao, 2021). In the self-coagulation, the recombination loss is a key factor, in contrast to the parabola theory (Lichtenberg, 1994; & Lichtenberg, 1997). The parabola profile at the discharge axis has been validated by the experiment (Berezhnoj, 2000; & Kaga, 2001). The superposed density bump and parabola profile occurred along the polar direction are not validated yet (Zhao, 2019; & Du, 2021). The flattened electron density needs to be checked as well, experimentally.

In the scope of this article, the self-consistent simulation and theory model construction of parabolic core profile, discharge separation, double layer,

and density bump of the electronegative discharge structure in the Ar/SF$_6$ plasma are concentrated. The article is outlined as follows. In Section II, the methods used are described, including the Ar/SF$_6$ plasma chemistry, inductive discharge chamber, fluid model, and analytical theory. In the Sections of III and IV, the results and discussion, and the conclusion and further remarks are given, respectively.

METHODOLOGY

Gas Chemistry

The gas-phase and surface chemical reactions of Ar/SF$_6$ plasma are given in Tabs. 1 and 2. The gas-phase chemistry includes the electron-impact reaction and the one happened between heavy species. The electron-impact reaction considers the cross section and reaction rate, two types. The cross section is taken from the lxcat database (Plasma, 2010) and integrated with the Maxwellian electron energy distribution function to generate the reaction rate. The other rates are directly taken from the References (Mao, 2011; & Yang, 2016). All these rates are applied in the continuity equations of fluid model. The surface reaction considers the recombination and de-excitation (Lallement, 2009; Mao, 2011; & Yang, 2016), as shown in Table. 2. In total, 24 plasma species are included, i.e., Ar, Ars (Metastable state atom), Ar+, SFx (x=1-6), SFy+ (y=1-5), SFz-(z=2-6), F+, F-, F2+ F2- and S+. In these species reactions, the ion-recombination reaction is found to play an important role in the self-coagulation behavior.

Inductive Discharge Chamber

The inductive discharge chamber used is schematically plotted in Figure. 1. As known, the inductively coupled plasma source is advantageous in the microelectronic industry application due to its characteristics such as the high plasma density generated at low pressure and simple equipment (Lieberman, 2005; & Chabert, 2011). So, it is important to study the discharge mechanism of this type of plasma. As shown in Figure 1, the chamber consists of matching box (for installing planar coil), dielectric window (for separating the discharge from coil), and the substrate (for etching and deposition). The chamber shape is cylinder and the axial symmetry is assigned. The height and radius of discharge chamber are 13 cm and 15 cm, respectively. The thickness of dielectric window is 1 cm and the height of matching box is 3 cm. Their radii are the same, 14 cm. The height and radius of substrate are 4 cm and 13 cm, respectively. In the simulation, the size and shape of two-turn coil are not considered and its interior and exterior turn radii are 6 cm and 8 cm, respectively. One 13.56 MHz radio frequency current source is connected to the coil to excite the inductive mode plasma. The background gas advection is not considered in the present work and the gas inlet and outlet nozzles are therefore not set.

Fluid model

The fluid model used is similar to the work of Reference (Zhao, 2018). It includes the equations of electron and heavy species, electromagnetic equation and the
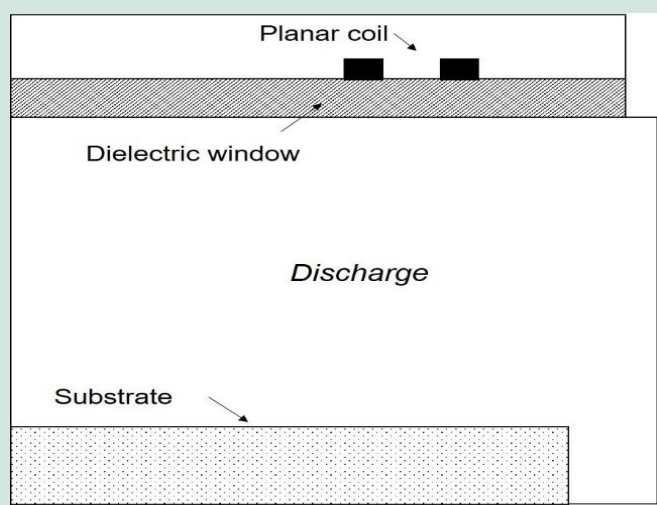

Figure 1: Configuration of inductive discharge chamber used in the fluid simulation.

Poisson's equation. The continuity and energy balance of electron are described by its equations and the drift and diffusion approximation is used for the momentum equation. The heavy species include the cation, anion and neutral particle, and they are described by the mass fraction equation. The energy balance is not addressed in the heavy species equation, and their thermal temperatures are unified as 300K, room temperature. The electromagnetic equation calculates the azimuthal electric field excited by the radio frequency electric current of coil, and then the field is deposited into the Ohm's heating source and transmitted into the electron energy equation as the power term. The Poisson's equation controls the ambi-polar diffusion process and it gives rise to the plasma potential and border sheath structure. The applicability of fluid model at the low pressure, i.e., 10 mTorr, is validated in Reference (Zhao, 2018), where the more detail of fluid model used is also given.

Analytical theory

The fluid simulation shows much detail of dynamic evolution of plasma. It is self-consistent and considers as much as possibly physical fields. Thus, it becomes difficult to analyze the physics occurred in the self-consistent simulation, due to the complicated interaction between so many fields (Lichtenberg, 1994; & Lichtenberg, 1997). From our experience (Zhao, 2021), the method for solving the problem is to examine the simulation and select out reasonable ingredients to construct equation. In searching of the equation solution, the behind physics covered in the simulation is picked. In the article, three theories formed in this means are given. They are axial parabola, polar parabola, and self-coagulation (Lichtenberg, 1994; Lichtenberg, 1997; & Zhao, 2021), shown in the Appendix A, Figure 2, and Appendix B, respectively. Besides, more detail of axial parabola theory can be referred to Figure S1 and Table. S1, in the supplementary material, and more detail of self-coagulation theory can be referred to Figure S2 and Table. S2, in the supplementary material as well.

The parabola theory shown in Appendix A and in the Figure S1 and Table. S1 of supplementary material is given by Lichtenberg et al (Lichtenberg, 1994).

For simplicity, the theory is deduced in the one-dimensional space. It is better used to explain the axial ion density profile simulated by fluid model in the cylindrical coordinate system. So, it is defined here as one axial parabola theory. Anion in the theory is assigned to satisfy the Boltzmann balance. It is the basis of theory construction. At the balance, the cation transport is depicted by the ambi-polar diffusion model, as the ion does in electropositive plasma. The ambi-polar diffusion coefficient deduced is complex function of electronegativity. At the approximation of high electronegivity and meanwhile considering the large discrepancy of electron and heavy ion mobilities, the coefficient is simplified significantly to be one constant. The electron density is flattened when anion is the Boltzmann balanced, i.e., the densities along the profile all equal to the centric density. By further assuming a negligible recombination loss, the parabolic profile of cation density is given by the continuity equation, at the homogeneous boundary condition of anion density of discharge separation location. In the appendix A, we still discussed the reasonability of using the Lichtenberg's models to interpret the discharge structure of electronegative inductively coupled plasmas, relative to the capacitive plasmas.

For further interpreting the polar ion density profile simulated, the polar parabola theory is given by us and shown in Figure 2. The polar theory is extended from the axial one on the basis of coordinate transform. The axial infinitely long cylinder model is assumed and the polar profile of electric potential at the fixed charge density is examined by the Poisson's equation. The solution is given by the Gaussian's law and the profile is coincidently a parabola. The similarity of cation continuity and the Poisson's equations is then used, as illustrated by the analogy method listed in Table. 3. Besides, the variables used in the formulae of Figure 2 are explained in the Table 3 as well.

At the above assumption, the potential distribution is a parabola, calculated by using the Gaussian's law of electrostatic theory. The variables used in the polar parabola theory are interpreted in Table 3, together with the detail of analogy method used.

The self-coagulation theory is deduced from the fluid simulation of an Ar/O2 inductively coupled plasma by

Table 1: Chemical reaction set considered in the model.

No.	Reaction	Rate coefficient[a]	Threshold (eV)
1	$e + Ar \rightarrow e + Ar$	Cross Section	0
2	$e + SF_6 \rightarrow e + SF_6$	Cross Section	0
3	$e + F_2 \rightarrow e + F_2$	Cross Section	0
4	$e + F \rightarrow e + F$	Cross Section	0
5	$e + Ar \rightarrow e + Ars$	Cross Section	11.6
6	$e + Ars \rightarrow e + Ar$	Cross Section	-11.6
7	$e + Ar \rightarrow 2e + Ar^+$	Cross Section	15.76
8	$e + Ars \rightarrow 2e + Ar^+$	Cross Section	4.43
9	$e + SF_6 \rightarrow SF_5^+ + F + 2e$	$1.2 \times 10^{-7} \exp(-18.1/T_e)$	16
10	$e + SF_6 \rightarrow SF_4^+ + 2F + 2e$	$8.4 \times 10^{-9} \exp(-19.9/T_e)$	20
11	$e + SF_6 \rightarrow SF_3^+ + 3F + 2e$	$3.2 \times 10^{-8} \exp(-20.7/T_e)$	20.5
12	$e + SF_6 \rightarrow SF_2^+ + F_2 + 2F + 2e$	$7.6 \times 10^{-9} \exp(-24.4/T_e)$	28
13	$e + SF_6 \rightarrow SF^+ + F_2 + 3F + 2e$	$1.2 \times 10^{-8} \exp(-26.0/T_e)$	37.5
14	$e + SF_6 \rightarrow F^+ + SF_4 + F + 2e$	$1.2 \times 10^{-8} \exp(-31.7/T_e)$	29
15	$e + SF_6 \rightarrow S^+ + 4F + F_2 + 2e$	$1.4 \times 10^{-8} \exp(-39.9/T_e)$	18
16	$e + SF_5 \rightarrow SF_5^+ + 2e$	$1.0 \times 10^{-7} \exp(-17.8/T_e)$	11
17	$e + SF_5 \rightarrow SF_4^+ + F + 2e$	$9.4 \times 10^{-8} \exp(-22.8/T_e)$	15
18	$e + SF_4 \rightarrow SF_4^+ + 2e$	$4.77 \times 10^{-8} \exp(-16.35/T_e)$	13
19	$e + SF_4 \rightarrow SF_3^+ + F + 2e$	$5.31 \times 10^{-8} \exp(-17.67/T_e)$	14.5
20	$e + SF_3 \rightarrow SF_3^+ + 2e$	$1.0 \times 10^{-7} \exp(-18.9/T_e)$	11
21	$e + F \rightarrow F^+ + 2e$	$1.3 \times 10^{-8} \exp(-16.5/T_e)$	15
22	$e + S \rightarrow S^+ + 2e$	$1.6 \times 10^{-7} \exp(-13.3/T_e)$	10
23	$e + F_2 \rightarrow F_2^+ + 2e$	$1.37 \times 10^{-8} \exp(-20.7/T_e)$	15.69
24	$e + SF_6 \rightarrow SF_6^-$	Cross Section	0
25	$e + SF_6 \rightarrow SF_5^- + F$	Cross Section	0.1
26	$e + SF_6 \rightarrow SF_4^- + 2F$	Cross Section	5.4
27	$e + SF_6 \rightarrow SF_3^- + 3F$	Cross Section	11.2
28	$e + SF_6 \rightarrow SF_2^- + 4F$	Cross Section	12
29	$e + SF_6 \rightarrow F^- + SF_5$	Cross Section	2.9
30	$e + SF_6 \rightarrow F_2^- + SF_4$	Cross Section	5.4
31	$e + F_2 \rightarrow F^- + F$	Cross Section	0
32	$e + SF_6 \rightarrow SF_5 + F + e$	$1.5 \times 10^{-7} \exp(-8.1/T_e)$	9.6
33	$e + SF_6 \rightarrow SF_4 + 2F + e$	$9.0 \times 10^{-9} \exp(-13.4/T_e)$	12.4
34	$e + SF_6 \rightarrow SF_3 + 3F + e$	$2.5 \times 10^{-8} \exp(-33.5/T_e)$	16
35	$e + SF_6 \rightarrow SF_2 + F_2 + 2F + e$	$2.3 \times 10^{-8} \exp(-33.9/T_e)$	18.6
36	$e + SF_6 \rightarrow SF + F_2 + 3F + e$	$1.5 \times 10^{-9} \exp(-26.0/T_e)$	22.7

No.	Reaction	Rate coefficient	
37	$e + SF_5 \rightarrow SF_4 + F + e$	$1.5\times10^{-7}\exp(-9.0/T_e)$	5
38	$e + SF_4 \rightarrow SF_3 + F + e$	$6.2\times10^{-8}\exp(-9.0/T_e)$	8.5
39	$e + SF_3 \rightarrow SF_2 + F + e$	$8.6\times10^{-8}\exp(-9.0/T_e)$	5
40	$e + SF_2 \rightarrow SF + F + e$	$4.5\times10^{-8}\exp(-9.0/T_e)$	8
41	$e + SF \rightarrow S + F + e$	$6.2\times10^{-8}\exp(-9.0/T_e)$	7.9
42	$e + F_2 \rightarrow 2F + e$	$1.2\times10^{-8}\exp(-5.8/T_e)$	1.6
43	$S + F \rightarrow SF$	2×10^{-16}	0
44	$SF + F \rightarrow SF_2$	2.9×10^{-14}	0
45	$SF_2 + F \rightarrow SF_3$	2.6×10^{-12}	0
46	$SF_3 + F \rightarrow SF_4$	1.6×10^{-11}	0
47	$SF_4 + F \rightarrow SF_5$	1.7×10^{-11}	0
48	$SF_5 + F \rightarrow SF_6$	1.0×10^{-11}	0
49	$SF_3 + SF_3 \rightarrow SF_2 + SF_4$	2.5×10^{-11}	0
50	$SF_5 + SF_5 \rightarrow SF_4 + SF_6$	2.5×10^{-11}	0
51	$SF + SF \rightarrow S + SF_2$	2.5×10^{-11}	0
52	$SF_x + F_2 \rightarrow SF_{x+1} + F$ [b]	7.0×10^{-15}	0
53	$X^+ + Y^- \rightarrow X + Y$ [c]	5.0×10^{-9}	0
54	$Z + Y^- \rightarrow Z + Y + e$ [d]	5.27×10^{-14}	0
55	$Ars + Ars \rightarrow e + Ar + Ar^+$	6.2×10^{-10}	0
56	$Ars + Ar \rightarrow Ar + Ar$	3.0×10^{-15}	0
57	$Ar^+ + SF_6 \rightarrow SF_5^+ + F + Ar$	9.0×10^{-10}	0
58	$SF_5^+ + SF_6 \rightarrow SF_3^+ + SF_6 + F_2$	6.0×10^{-12}	0

[a] The unit of the rate coefficient is cm³s⁻¹.
[b] x stands for the number 1-5.
[c] $X = SF_5$、SF_4、SF_3、SF_2、SF、F、S or F_2 and $Y = SF_6$、SF_5、SF_4、SF_3、SF_2、F or F_2.
[d] $Z = SF_6$、SF_5、SF_4、SF_3、SF_2、SF、F、S or F_2 and $Y = SF_6$、SF_5、SF_4、SF_3、SF_2、F or F_2.

Table 2: Surface reaction set considered in the model

No.	Surface reaction	Sticking coefficient
1	$e + Ar \rightarrow e + Ar$; $x = 1-5$	1
2	$e + F_2 \rightarrow e + F_2$	1
3	$e + F \rightarrow e + F$	1
4	$e + Ar \rightarrow e + Ars$	1
5	$e + Ars \rightarrow e + Ar$	0.02
6	$Ar^+ + wall \rightarrow Ar$	1
7	$Ars + wall \rightarrow Ar$	1

Table 3: The symbols and their corresponding physical quantity names of Figure 2 and the detail of analogy method used.

Symbol	Physical quantity	Notes
$2D_+$	Simplified ambi-polar diffusion coefficient	
k	Ionization rate coefficient	
G_0	Generation rate of cation	
$\vec{\Gamma}_+$	Flux of cation	For the continuity equation
n_+	Density of cation	
$r, \theta, z,$	Independent variables of continuity equation in cylindrical coordinate	
ρ_0	Constant charge density	Solving the Poisson's equation by means of the Gaussian's law.
ε	Dielectric constant	$S_r = 2\pi r dr \cdot dl,$
$q_{i,interior}$	Charge amount surrounded by enclosed surface	$q_{i,interior} = \pi r^2 \cdot dl,$
S	Area of enclosed surface	$\oiint \vec{E} \cdot d\vec{s} = E_r \cdot S_r \ (E_z = 0).$
Analogy method	$\vec{\Gamma}_+ \sim \vec{E}$ $\Gamma_{+,r} \sim E_r$ $G_0 \sim \rho_0$ $\varphi \sim n_+$	Similarity: $\varphi = -\dfrac{\rho_0}{4\varepsilon} r^2 + A_{const},$ $n_+ = -\dfrac{G_0}{8D_+} r^2 + B_{const}.$

Figure 2: Our polar parabola theory. In panel (a), the cation continuity equation is given, at the assumption of an axial symmetric, infinitely long cylinder. At the assumption, only the polar component of cation flux exists. In panel (b), the Poisson's equation with the same expression as the continuity equation is displayed.

us in Reference (Zhao, 2021), at axial symmetry. The simulation shows a strong accumulation of anion at the top of ambi-polar diffusion potential, and the chemical source of anion there is negative for the recombination is dominated. The free-diffusion and negative source of anion continuity equation are sampled to construct the quasi-Helmholtz equation. The test solution of equation is given by the method of separation of variable. It is just a spatially independent delta function, which mathematically interprets well the occurrence of self-coagulation process. Besides, we added a detailed discussion on deducing the self-coagulation theory, in

Appendix B of the present article and in the Figure S2 and Table S2 of supplementary material. The behind physics of self-coagulation is further searched by means of one equivalent spring oscillator that works at a dispersing force (not retrieving), e.g., gravitation. More detail of the model can be found in Reference (Zhao and Li, 2021).

RESULTS AND DISCUSSION

Discharge Separation

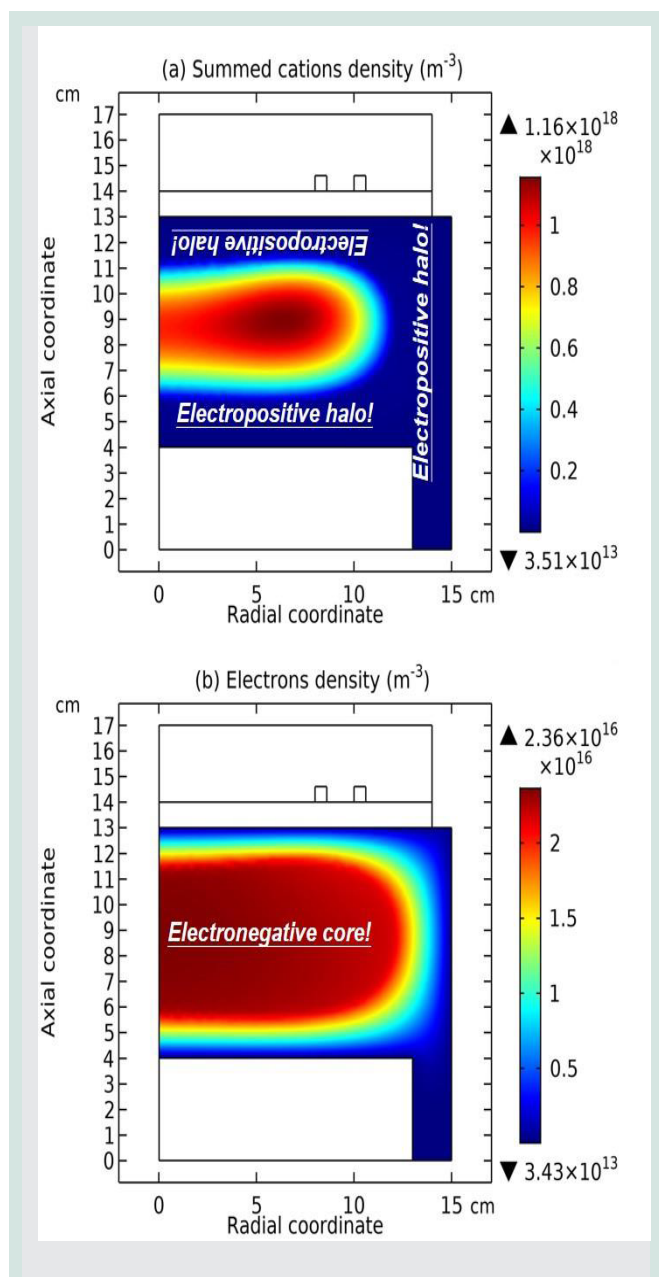In Figure 3, the two dimensional profiles of simulated cation density sum and electron density are plotted,

Figure 3: Density profiles of the summed cations (a) and electron (b) in the Ar/SF$_6$ inductively coupled plasma given by fluid simulation, at the discharge condition of 300W, 10mTorr and 10% SF$_6$ content.
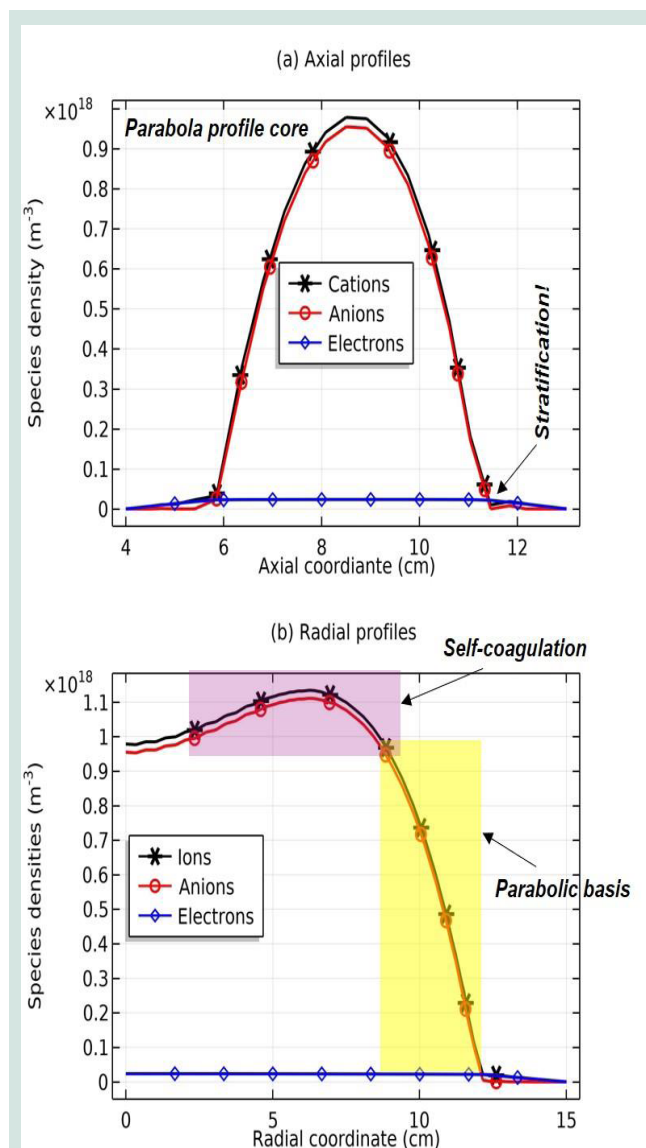
Figure 4: Axial (a) and polar (b) profiles of the summed cations and anions densities, and the electron density in the Ar/SF$_6$ inductively coupled plasma simulated by fluid model, at the discharge condition of 300W, 10mTorr and 10% SF$_6$ content.

at the discharge condition of 300W, 10mTorr and the 9:1 Ar vs. SF$_6$ gas content ratio. In Figure 4, the axial and polar density profiles of summed cations, summed anions and electron are given, at the same discharge condition. In Figure 5, the charge density of this Ar/SF$_6$ plasma is shown. Clear border is seen from the profiles, where the summed cation and anion densities are both truncated and meanwhile the strong non- electric neutrality is appeared. In the region surrounded by the border, both of the cation and anion densities are high and meanwhile the electron density (more or less two orders lower than the two ions) profile is flat. The electron density in the exterior of the border is smoothly descended, which is neutralized by the cations. The border separates the discharge into two parts, i.e., Electronegative Core that consists basically of cation and anion in the interior of border and Electropositive Edge that consists mainly of electron and cation (edge can be re-named as halo upon thinking of the cylindrical shape of chamber) in the exterior of border. The discharge separation was early revealed by the analytical theory, called as the discharge stratification in the history (Lichtenberg, 1994; Lichtenberg, 1997; Economou, 2007; & Lampe, 2004). In the present article, it is first reported by means of a fluid simulation. Meanwhile, we renamed it as a discharge separation phenomenon, aimed at distinguishing it from the discharge striations that happen in the capacitively coupled electronegative plasma (Liu, 2016). These two mechanisms are clearly not the same and hence better to be named distinguishingly.

Parabola Profile and Theory

As seen in Figure 4 (a), the axial profile of summed cations density in the core plotted at the discharge center is basically a parabola profile. As stated, the parabola profile simulated is determined by the parabola theory given in the Appendix A and in the Figure S1 and Table S1 of supplementary material. In the parabola theory, the recombination loss in the continuity equation is assumed to be negligible. This is verified by the fluid simulation. The net sources of cation at both the 10mTorr and 90mTorr are shown in Figure 6. At 10mTorr, the net source is indeed dominated by ionizations, while at 90mTorr the ionizations are counteracted by recombinations (where a flat-top model other than the parabola prevails (Lichtenberg, 1997)). One more approximation of the parabola theory is captured by the fluid simulation, i.e., the anion Boltzmann balance, given in Figure 7. In the figure, the potential of core is seen to be flat at a macroscopic level (i.e., observed within the range of ambi-polar diffusion potential), but is spatially varied upon being zoomed into (see Figure 7(b)), at the anion room temperature magnitude. The Boltzmann relation is proven via the curve similarity of normalized anion
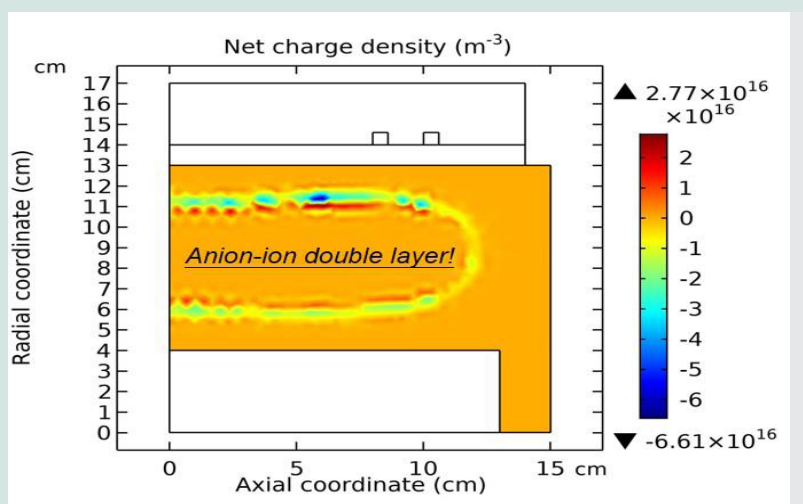

Figure 5: Charge density profile of the Ar/SF$_6$ plasma given by the fluid simulation. The discharge condition is the same as in Figures. 3 and 4.
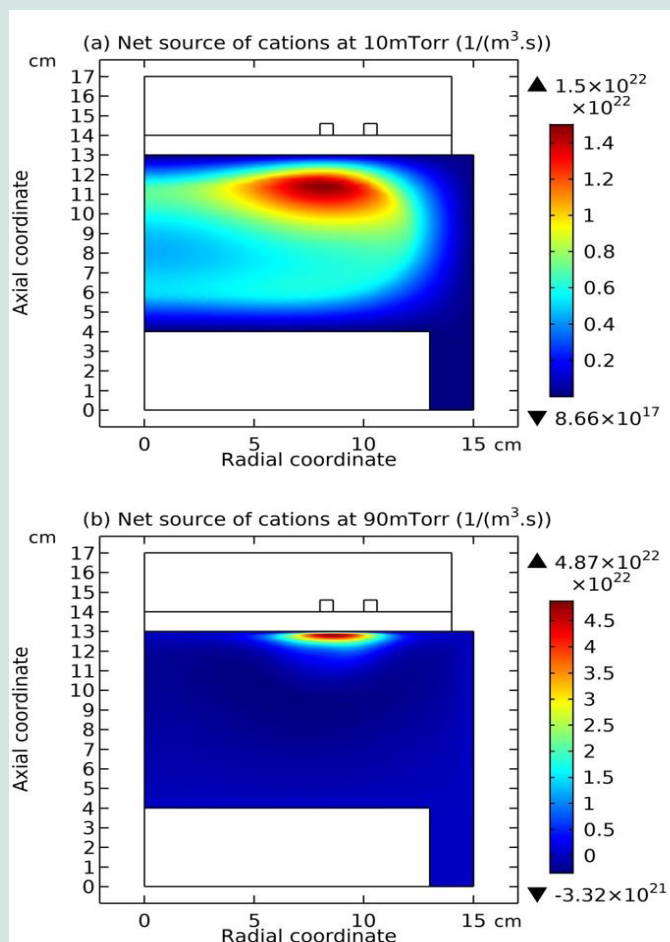
Figure 6: Net source of cation in the Ar/SF6 plasma at (a) 10mTorr and (b) 90mTorr, given by the fluid simulation at the other discharge condition, 300W and 10% SF_6 content.
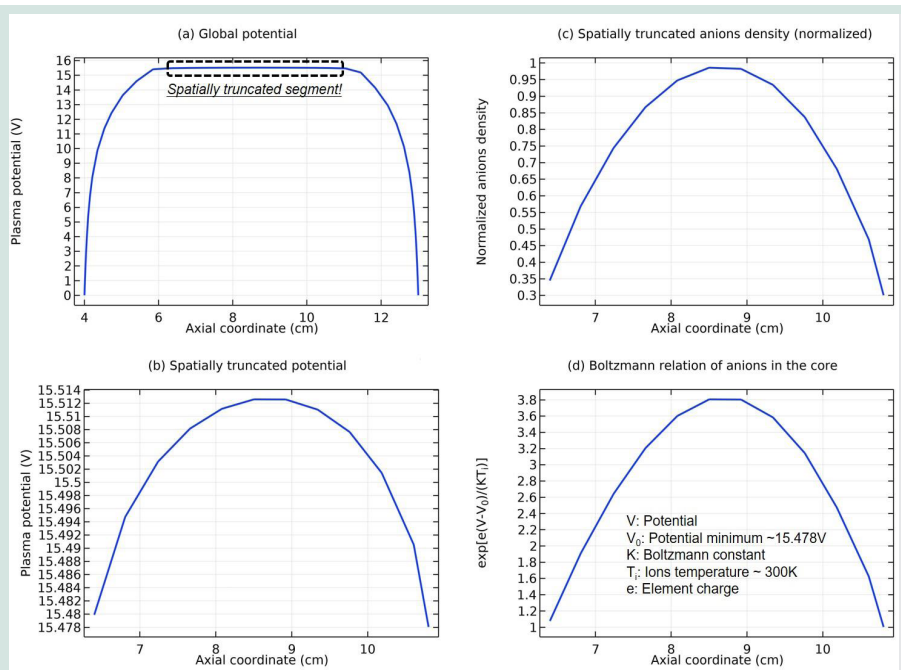

Figure 7: The Boltzmann's relation of anion in the electronegative core when the basic discharge structure is separated, at the same discharge condition as in Fig. 3. In (a), the global axial plasma potential is exhibited. In the central flattened part, i.e., the core, a path of potential is segmented. In the segment, the tiny variation of potential (b), normalized anion density (c) and the Boltzmann equilibrium of anion with potential (d) are sequentially shown. The discrepancy in the magnitudes of (c,d) is ascribed to the robust truncation operation, and it is believed to not influence the reasonability of the anion Boltzmann equilibrium. In the present fluid model, the temperatures of cations and anion are both assumed to be room temperature.

density and exponential function of the potential difference over anion temperature, as shown in Figure 7(c,d). Theoretically, it forms a Boltzmann balance, just exhibited by means of the simulation. Since both the electron and anion satisfy the Boltzmann balance, the core electron density simulated in Figure 3(b) is flat, as determined also by the parabola theory in the Appendix A and in the Figure S1 and Table S1 of supplementary material.

Self-coagulation of Anion and Density Bump

As seen in Figure 4(b), along the polar direction, the anion density profile simulated exhibits the superposition of parabola basis (determined by the parabola theory of polar direction shown in the Figure 2 of Sec. II) and a density bump. As told before, the density bump is given by the self-coagulation process and the related theory is introduced in the Appendix B and in the Figure S2 and Table S2 of supplementary material.

In the self-coagulation theory, the transport of free diffusion and the chemical source of recombination dominance are needed. The two requirements are met in the Ar/SF_6 plasma. As seen in Figure 8, the negative source of anion at the density bump position is produced in the simulation. In addition, the flat potential profile of core shown in Figure 7(a) ensures the free diffusion transport of anion. Although the anion is still Boltzmann balanced, the free diffusion is talked about in the scope of ambi-polar diffusion potential level (rather higher than ions temperature), and so this balance over the room temperature does not influences the self-coagulation behavior. In a word, the Boltzmann-balanced anion assists the cation to generate the parabola basis, while the freely-diffusing anion directly generates the density bump. The interesting dual character of anion discussed here, we believe, is a result of the non-thermal equilibrium
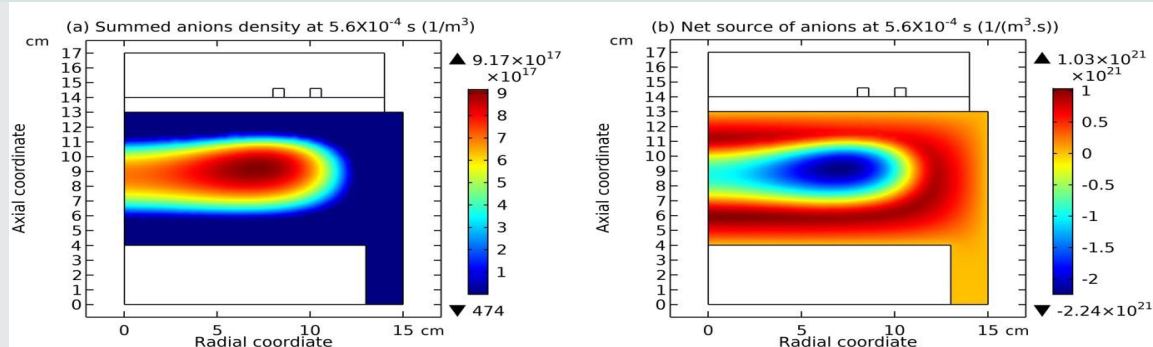

Figure 8: Summed anions density (a) and their net source (b) in the Ar/SF_6 plasma, given by the fluid model at the discharge condition of 300W, 10mTorr and 10% SF_6 content.
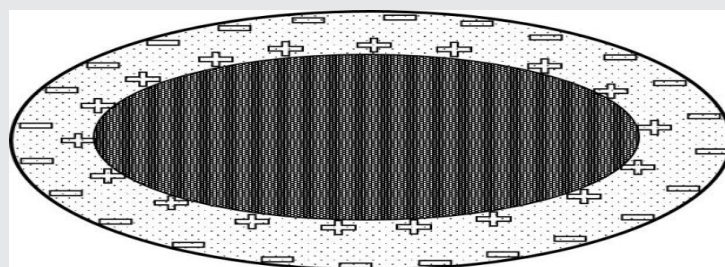

Figure 9: The equivalent ellipsoid capacitor of dielectric-type double layer, discovered in fluid simulation of the Ar/SF_6 inductively coupled plasma

property of laboratory plasma.

Dielectric-type Double Layer

In Figure 5, the two layers of charge with different polarities are seen at the interface of electronegative core and electropositive edge, called as double layer. Early works define the double layer as potential step (Quon, 1976; Coakley, 1978; Knorr, 1974; Chan, 1984; & Chan, 1986). It is described as a result of two thin layers with different polarities, given by the Poisson's equation in Reference (Quon, 1976). It is noted that the potential step and the two layers are both predicted by the fluid simulation. See Figure 7(a) for the potential step and Figure 5 for the two charge layers.

Next, we address why the double layer is appeared and its essence. Laboratory plasma is bounded plasma, and the building of steady-state laboratory plasma from the gas-breakdown initial state is a very fast process. Strong source exists in the short duration. In a plasma medium, the source induces the ambi-polar diffusion mode and in the transport means, electron is the Boltzmann balanced. Furthermore, in the electronegative laboratory plasma at low pressure, anion is also the Boltzmann balanced (Lichtenberg, 1997) (see before). This implies that the electron and anion of laboratory plasma hardly flow at the above equilibrium. So, there are no charge carriers and electric current is thereby not easily formed, which indicates the dielectric property of laboratory plasma. On contrast, space plasma is unbounded plasma and always evolves at large time scale. The source is not important and ambi-polar diffusion is not existed. So, space plasma is full of free charge carriers and it is therefore treated as conductor. Due to this distinction, the space plasma double layer is always triggered by stream instability. Correspondingly, the double layer of laboratory plasma is one dielectric-type. Concretely, At the discharge initial, the ambi-polar diffusion potential is formed at the chamber border, and then at high enough electronegativity, the pair plasma of cation and anion is faced with the potential difference. Due to its dielectric character, the pair plasma is polarized to form a capacitor. Considering the chamber and plasma structure, the formed capacitor is more like an ellipsoid, as shown in Figure 9. Inductively coupled plasma behaves

more like a direct current (DC) plasma, so the dielectric double layer blocks the inward movement of ambi-polar diffusion potential of exterior which carries the electric current of cation (cation is drifted in the ambi-polar diffusion). The interior plasma part surrounded by the capacitor therefore has to find its own way to get to the balance. So, the discharge is separated, by the double layer. It is noted that the formation of dielectric double layer requires high enough electronegativity to ensure the existence of dielectric pair plasma of ions. This probably can explain why Hershkowitz et al failed to find the double layer in a mixed Ar-O2 plasma (with the low electronegativity) in Reference (Kim, 2009).

CONCLUSION

In this work, the discharge structure of an Ar/SF6 inductively coupled plasma is investigated by means of both the fluid simulation and analytic theory, at low pressures. The discharge separation revealed by the analytical theory (previously called as discharge stratification) is the first time reported by a self-consistent simulation. The separation is led to by the dielectric-type double layer, which makes it possible to realize two types of transport mode in one plasma source. The parabolic profile simulated is in good accordance to the parabola theory. Anion holds the double identities due to the non- thermal equilibrium property of laboratory plasma. The Boltzmann's balance of anion is necessary for the parabola theory, and meanwhile the self-coagulation needs the attendance of anion that is freely diffused. The two processes give rise to the case of discharge profile superposition. To fully recognize the discharge structure, the more experimental validation of simulation and theory discovery is still needed and being carried out.

The discharge separation is more predominant at relatively low pressures because the diffusion and mobility coefficients of plasma species, i.e., electron, cation and anion, are high and hence the ambi-polar diffusion potential is easily built, which, once executed on the pair plasma of ions, will polarize it and generate the double layer. At increasing the pressure, the separating border is moved to the chamber periphery, almost connecting to the chamber border sheath. The simulated trend is again in accordance to the theory

prediction of Reference (Lichtenberg, 1997). The more detail of inductively coupled plasma discharge structure with high electronegativity at high pressures will be given in a future work.

CONFLICT OF INTEREST

The authors have no conflicts to disclose.

DATA AVAILABLE STATEMENT

The data that support the findings of this study are available within the article.

ONLINE SUPPLEMENTARY MATERIAL

The supplementary material-More detail of analytic theory is provided, where more details of parabola and self-coagulation theories are given.

REFERENCE

- Albert, R. D., & Lindstrom, P. J. (1970). Auroral-particle precipitation and trapping caused by electrostatic double layers in the ionosphere. *Science, 170*(3965), 1398-1401. https://doi.org/10.1126/science.170.3965.1398

- Berezhnoj, S. V., Shin, C. B., Buddemeier, U., & Kaganovich, I. (2000). Charged species profiles in oxygen plasma. *Appl. Phys. Lett., 77*(6), 800-802. https://doi.org/10.1063/1.1306637

- Bogdanov, E. A., Kudryavtsev, A.A., & Ochikova, Z.S. (2013). Main Scenarios of Spatial Distribution of Charged and Neutral Components in SF_6 plasma. *IEEE Trans. Plasma Sci., 41*(12), 3254-3267.

- Chabert, P., & Braithwaite, N. (2011), *Physics of radio-frequency plasmas.* Cambridge University Press. Cambridge.

- Chan, C., Cho, M. H., Hershkowitz, N., & Intrator, T. (1984). Laboratory evidence for ion-acoustic-type double layers. *Phys. Rev. Lett., 52*(20), 1782-1785. https://doi.org/10.1103/PhysRevLett.52.1782

- Chan, C., Cho, M. H., Hershkowitz, N., & Intrator, T. (1986). Experimental observation of slow ion acoustic double layers. *Phys. Rev. Lett., 57*(24), 3050-3053. https://doi.org/10.1103/PhysRevLett.57.3050

- Coakley, P., Hershkowitz, N., Hubbard, R., & Joyce, G. (1978). Experimental observation of strong double layer. *Phys. Rev. Lett., 40*(4), 230-233. https://doi.org/10.1103/PhysRevLett.40.230

- Du, P. C., Gao, F., Wang, X. K., Liu, Y. X., & Wang, Y. N. (2021). Measurement of electronegativity during the E to H mode transition in a radio frequency inductively coupled Ar/O_2 plasma. *Chin. Phys. B, 30*(3), 035202. https://doi.org/10.1088/1674-1056/abccb0

- Economou, D. J. (2007). Fundamentals and applications of ion-ion plasmas. *Appl. Surf. Sci., 253*(16) 6672-6680. https://doi.org/10.1016/j.apsusc.2007.02.004

- Kaga, K., Kimura, T., Imaeda, T., & Ohe, K. (2001). Spatial structure of electronegative Ar/CF_4 plasmas in capacitive RF discharges. *Jpn. J. Appl. Phys., 40*(10), 6115-6116. https://doi.org/10.1143/JJAP.40.6115

- Kim, Y. C. & Hershkowitz, N. (2009). Experimental verification of Boltzmann equilibrium for negative ions in weakly collisional electronegative plasmas. *Appl. Phys. Lett., 94*(15), 151503. https://doi.org/10.1063/1.3119627

- Knorr, G. & Goertz, C. K. (1974). Existence and stability of strong potential double layers. *Astrophys. Space Sci., 31*(1), 209-223. https://doi.org/10.1007/BF00642612

- Kolobov V. I. & Economou, D. J. (1998). Ion-Ion plasmas and double layer formation in weakly collisional

electronegative discharges. *Appl. Phys. Lett., 72*(6), 656-658. https://doi.org/10.1063/1.120837

- Kouznetsov, I. G., Lichtenberg, A. J., & Lieberman, M. A. (1999). Internal sheaths in electronegative discharges. *J. Appl. Phys., 86*(8), 4142-4153. https://doi.org/10.1063/1.371339

- Lallement, L., Rhallabi, A., Cardinaud,C., Peignon-Fernandez, M. C., & Alves, L. L. (2009). Global model and diagnostic of a low-pressure SF_6/Ar inductively coupled plasma. *Plasma Sources Sci. Tech., 18*(2), 025001. https://doi.org/10.1088/0963-0252/18/2/025001

- Lampe, M., Manheimer, W. M., Fernsler, R. F., Slinker, S. P., & Joyce, G. (2004). The physical and mathematical basis of stratification in electronegative plasmas. *Plasma Sources Sci. Technol., 13*(1), 15-26. https://doi.org/10.1088/0963-0252/13/1/003

- Lieberman, M. A. & Lichtenberg, A. G. (2005). *Principles of plasma discharges and materials processing.* Wiley. New York.

- Lichtenberg, A. J., Kouznetsov, I. G., Lee, Y. T., Lieberman, M. A., Kaganovich, I. D., & Tsendin, L. D. (1997). Modelling plasma discharges at high electronegativity. *Plasma Sources Sci. Technol., 6*(3), 437-449. https://doi.org/10.1088/0963-0252/6/3/022

- Lichtenberg, A. J., Vahedi V., Lieberman, M. A., & Rognlien, T. (1994). Modelling electronegative plasma discharges. *J. Appl. Phys., 75*(5), 2339-2347. https://doi.org/10.1063/1.356252

- Liu, Y. X., Edmund, S., Ihor, K, Zoltan, D., & Wang, Y. N. (2016). Experimental observation and computational analysis of striations in electronegative capacitively coupled radio-frequency plasma. *Phys. Rev. Lett., 116*(25), 255002. https://doi.org/10.1103/PhysRevLett.116.255002

- Mao, M., Wang, Y. N., & Bogaerts, A. (2011). Numerical study of the plasma chemistry in inductively coupled SF_6 and SF_6/Ar plasmas used for deep silicon etching applications. *J. Phys. D: Appl. Phys., 44*(43), 435202. https://doi.org/10.1088/0022-3727/44/43/435202

- Plasma Data Exchange Project. [Online]. Available:[EB/OL]. https://fr.lxcat.net/instructions/, built in 2010.

- Quon B. H. & Wong A. Y., (1976). Formation of potential double layers in Plasmas. *Phys. Rev. Lett., 37*(21), 1393-1396. https://doi.org/10.1103/PhysRevLett.37.1393

- Schulze, J., Derzsi, A., Dittmann, K., Hemke, T., Meichsner, J., & Donko, Z. (2011). Ionization by drift and ambipolar electric fields in electronegative capacitive radio frequency plasmas. *Phys. Rev. Lett.,107*(27), 275001. https://doi.org/10.1103/PhysRevLett.107.275001

- Sheridan, T. E. (1999). Double layers in a modestly collisional electronegative discharge. *J. Phys. D: Appl. Phys., 32*(15), 1761-1767. https://doi.org/10.1088/0022-3727/32/15/301

- Vender, D., Stoffels, W. W., Stoffels, E., Kroesen, G. M. W., & Hoog, F. J. (1995). Charged-species profiles in electronegative radio-frequency plasma. *Physical Review E, 51*(3), 2436-2444. https://doi.org/10.1103/PhysRevE.51.2436

- Yang, W., Zhao, S. X., Wen, D. Q., Liu, W., Liu, Y. X., Li, X. C., & Wang, Y. N. (2016). F-atom kinetics in SF_6/Ar inductively coupled plasmas. *J. Vac. Sci. Tech. A, 34*(3), 031305. https://doi.org/10.1116/1.4945003

- Zhao, S. X. (2021). Quasi-delta negative ions density of Ar/O_2 inductively coupled plasma at very low electronegativity. *Chin. Phys. B, 30(5)*, 055201. https://doi.org/10.1088/1674-1056/abd16a

- Zhao, S. X. (2018). Non-monotonic behavior of electron temperature in argon inductively coupled plasma and its analysis via novel electron mean energy equation. *Phys. Plasmas, 25*(3), 033516. https://doi.org/10.1063/1.5012053

- Zhao, S. X. & Li, J. Z. (2021). Delta distribution of electronegative plasma predicted by reformed spring oscillator dynamic equation with dispersing force. *Chin. Phys. B, 30*(5), 055202. https://doi.org/10.1088/1674-1056/abd166

- Zhao, Y. F., Zhou, Y., Ma, X. P., Cao, L. Y., Zheng, F. G., & Xin, Y. (2019). Axial diagnosis of electron and negative ion behaviors in capacitively coupled O_2-containing Ar plasma driven by 27.12 MHz. *Phys. Plasmas, 26*(3), 033502. https://doi.org/10.1063/1.5079256

GLOBAL OPEN ACCESS JOURNAL OF SCIENCE